Creath: Choosing a phase-measurement algorithm for measurement of coated LIGO optics

Wednesday, February 10, 2021 4:20 PM

2000_KC_SPIE_vol41...

Choosing a phase-measurement algorithm for measurement of coated LIGO optics

Katherine Creath*
Optineering, Tucson, AZ 85719-6018

ABSTRACT

High precision measurements of nearly flat highly reflective surfaces present many problems when using a phase-measuring Fizeau interferometer. Since a coated reference surface is required to yield good fringe contrast with a high reflectance test surface, the interference fringes are likely to deviate from being perfectly sinusoidal. Utilizing phase-measurement algorithms that take data over a 2-wavelength range of phase shifter motion can help reduce the effects of errors due to non-sinusoidal fringes. If linear and 2nd-order phase shifter errors are present, the greater number of frames of fringe data can aid in making a better estimate of the phase. Eight algorithms that have been published in the literature are compared using simulations and experimental measurements. From this study, it was determined that a 12-frame algorithm having 60° ($\pi/3$) phase shifts developed by Surrel had superior performance when used with a Clapham-Dew type coated reference surface and a high reflectance test surface. Residual errors in the phase calculation were found to be reducible to a few thousandths of a wave peak-to-valley.

Keywords: Interferometry, interferometers, optical testing, optical metrology, phase measurement.

1. INTRODUCTION

The optics for the LIGO project have surfaces with long radii of curvature that need to be precisely measured.[1-3] Additionally, many of these optics have multi-layer dielectric high reflectance coatings designed to operate at 1064 nm. The challenge of measuring these surfaces led to making modifications on an existing commercially-available interferometer model. A Fizeau-type interferometer was specified because of its ease of use and availability. When measuring high reflectance surfaces using an uncoated reference surface, the fringe contrast is poor and the noise in the measurement increases substantially if it can at all even be measured. Thus, some type of coating needs to be used on the reference surface to increase the fringe contrast. The type of coating chosen for this task was a Clapham-Dew type coating that enables the reference surface to be used in either the reference or test positions.[4] The downside of using a coated reference surface is the likelihood that the interference fringes would be a bit non-sinusoidal. For many types of measurements, a slightly non-sinusoidal fringe isn't going to make a difference. However, for high precision measurements on surfaces with a residual rms of a nanometer or less, non-sinusoidal fringes can cause artifacts in the phase calculation. Thus, finding an appropriate phase measurement algorithm for the task was important.

A plethora of new algorithms and means of generating these algorithms has emerged in the literature in the last few years (for example Refs. 5-10). Rather than go to the drawing board and develop a new algorithm, the literature was mined for possible algorithms that were compared using simulations and then with experimental measurements to determine which ones minimized the expected sources of error. The types of algorithms that could be easily implemented in the existing software are comprised of arctangent calculations with polynomials in the numerator and denominator of sine and cosine terms respectively. The coefficients of these polynomials act as filtering functions for sampling the sine and cosine functions.[5]

For this study eight algorithms were compared having either 90° ($\pi/2$) or 60° ($\pi/3$) phase shifts and required a total range of the phase shifter between one and two wavelengths. The behavior of these algorithms was studied for linear and 2nd-order phase shifter errors as well as using simulated data for the anticipated fringe shape for measurements with the Clapham-Dew coated reference flat versus a high reflectance test surface. This paper outlines the simulations, their results and the experimental verification of the algorithm choice.

* Correspondence: Email: kcreath@ieee.org. The author is a consultant to the LIGO project of the California Institute of Technology in Pasadena, CA.

In *Laser Interferometry X: Techniques and Analysis*, Malgorzata Kujawińska, Ryszard J. Pryputniewicz, Mitsuo Takeda, Editors, Proceedings of SPIE Vol. 4101 (2000) • 0277-786X/00/$15.00

2. INTERFEROMETER SYSTEM

The LIGO project has involved many laboratories around the world in developing optics and testing procedures. The 250 mm diameter optical surfaces for the test masses and beamsplitters in the resonant cavity were manufactured by CSIRO in Australia. For this project CSIRO developed a Fizeau interferometer with a 300 mm aperture using a laser diode source[11] as well as a technique for calibrating this instrument.[12-15] Many of the uncoated surfaces were also measured at NIST with a 150 mm aperture Wyko 6000 operating at 633 nm.[16] Neither of these laboratories was set up to measure coated surfaces or to measure the finished optics at the wavelength of use (1064 nm). During the initial pathfinder phase of the project, a surface made by HDOS in Danbury MA was measured by HDOS,[17] NIST, and CSIRO. This surface has been used as a benchmark for performance for metrology of the LIGO optics at the California Institute of Technology.[18]

The task for this part of the project was to specify an interferometer to make measurements on the finished, coated optics and to get the system calibrated and develop measurement procedures. The goal was to compare surfaces before and after coating. The specifications of the surfaces to be measured as well as measurements on the uncoated surfaces are detailed in papers by Walsh et al. of CSIRO.[2,19-21] The test surfaces are flats or have ROCs (radii of curvature) from 7.4 km to 14.5 km that need to be known accurately to ±220 m and repeatably to ±110 m. Reflectivities vary from bare glass to 100%. Spatial scales of interest are 10 cm down to 1 mm for a 150 mm measurement area. Focus and astigmatism need to be known to λ/100 P-V (peak-to-valley). The residual rms after removing focus and astigmatism (as well as tilt and piston) terms needs to be known to λ/1000 rms over the full field of view. And the retrace error needs to be less than 3 nm P-V for 4 fringes tilt.

A commercially-available interferometer with simple modifications was desired both for economic reasons and for ease of use. For this work, a Wyko 6000 Fizeau interferometer operating at 1064 nm was utilized to measure 150 mm diameter areas. Instead of using a zoom lens, two image sizes were specified for 1X and 6X magnifications with a fixed focus location. The PZT's (piezo-electric transducers) used for shifting the reference surface had a long enough throw to take data with optical path differences up to 3 wavelengths. The long throw PZT's were specified so that phase-measurement algorithms using a larger number of frames of data could be used to reduce errors owing to expected non-sinusoidal fringe data. The software controlling the data taking had the ability to program in different phase measurement algorithms. Otherwise, the system was a standard configuration with a silicon analog CCD. A rough schematic of the Fizeau interferometer is shown in Fig. 1.

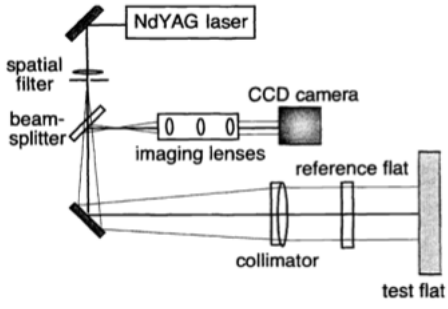

Figure 1. Rough schematic of Fizeau interferometer.

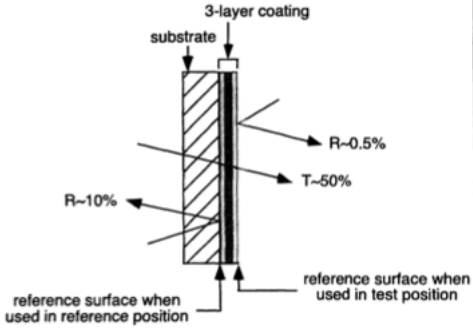

Figure 2. Reference surface with 3-layer Clapham-Dew coating with performance specifications.

To measure high reflectance surfaces, it was decided to use a Clapham-Dew type reference surface on the interferometer.[4] This type of coating enables high fringe contrast and minimizes multiple reflections as well as allowing the flat to be used in either the reference or test positions of the interferometer. (The coatings were designed, deposited and characterized by CSIRO.)[22,23] The design was a 3-layer stack (dielectric/absorber/dielectric) having 10% reflectance off the back side of the

coating, 50% transmittance and 0.5% reflectance off the front side of the coating (see Fig. 2). This reference surface design provides a fringe contrast of 0.95 when testing a flat with 100% reflectance, 0.5 testing an uncoated flat and 0.5 when this flat is used in the test position instead of the reference position. Data from thin films design software shows that the fringes will be noticeable non-sinusoidal. A concern in the implementation of the coating was variations in the thickness of the coating causing differences between measurements made with the reference flat in the reference and test positions. (These test techniques will be described in a subsequent paper.)[18] This situation could affect the results of 3-flat tests because the surface doing the reflecting is different when the flat is used in the two positions (see Fig. 2). Experimental observations confirmed this concern. Because of this, special care was made to find and develop test techniques that did not use this reference surface in the test position. It should be noted that the difference between the reflecting surfaces for the reference and test positions can be accounted for by characterizing the thickness variations of the coating.[23]

Simulations of the interference pattern expected between a reference surface with a Clapham-Dew type coating and a highly reflective test surface are shown in Fig. 3.[24] Irradiance for 4 different values of front surface reflectance are plotted versus one fringe worth of optical path difference (OPD) in nm. As the reflectance of the front surface increases so does the variation of the fringe data relative to a sinusoid. Figure 4 shows the difference between the expected fringe contour and a sine wave. Note that the variation for 0.15% reflectance is within a few percent irradiance of the sine wave. When the reflectance is 0.45%, the expected variation is about 10%.

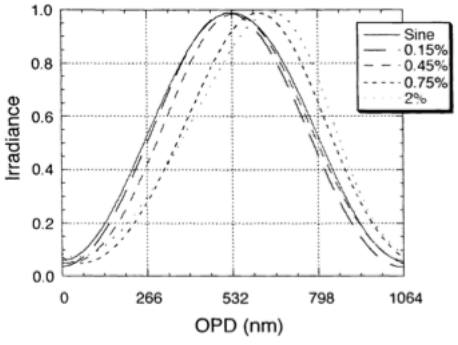

Figure 3. Calculated interference fringe irradiance for reference surface coating with different front surface reflectances versus one fringe of OPD.

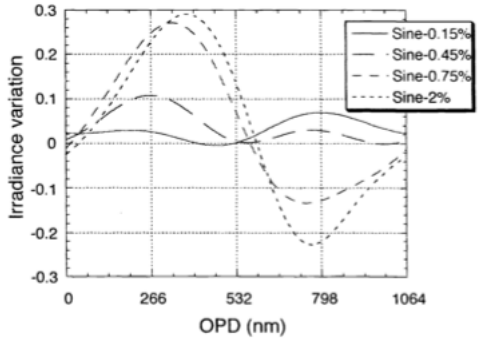

Figure 4. Difference between calculated fringe irradiance and a sinusoidal interference fringe versus OPD for different front surface reflectances.

3. PHASE-MEASUREMENT ALGORITHMS FOR SIMULATIONS

A major consideration in choosing a phase-measurement algorithm for this application was to minimize the error for measuring non-sinusoidal fringes. A second consideration was to find an algorithm that could also handle some error in the phase shift calibration. The long throw PZT's are not as linear as shorter throw PZT's. Because of measurement specifications (expectations of surfaces with 1 nm rms or better), high precision measurements were necessary and the error due to the phase measurement algorithm needed to be on the order of a few thousandths of a wave peak-to-valley (P-V). Essentially, the search was on for an algorithm insensitive to the irradiance variations that were expected to be present.

A number of different algorithms were tried on a standard Wyko interferometer operating at 633 nm using a Clapham-Dew reference flat and a highly reflective test surface. It was found that the algorithms which could be implemented on PZT's with a total throw of about 1 micrometer all had noticeable ripple present when tilt fringes were introduced in this configuration. The LIGO surfaces were expected to have 2-3 circular fringes present across the field of view owing to the long radii of curvature. Thus, ripple artifacts would be present in the measured surface profiles when the fringes were non-sinusoidal unless an appropriate algorithm was found.

To evaluate different phase-measurement algorithms. the data shown in Fig. 3 were used in simulations. A perusal of the literature revealed that the ripples could be reduced using algorithms that took data over 2-waves of OPD.

Eight phase-measurement algorithms were compared for this paper. Four of them had phase shifts of $\pi/2$ (90°) and the other four had phase shifts of $\pi/3$ (60°). For comparison of performance, one algorithm having one wave of OPD from the total phase shift was compared for each phase shift with 3 algorithms having close to two waves of OPD shift. More algorithms were tested than will be reported in this paper. After sifting through the available literature and testing a number of algorithms it was found that many of the published algorithms had mistakes in them and others could not easily be implemented. For two of the algorithms used in this study, corrections to the equations were easily obtained from the authors who developed them.

The algorithms compared are shown in Eqs. (1)-(8).

5-frame 90° [25,26]
$$\phi = \tan^{-1}\left[\frac{2(I_2 - I_4)}{I_1 - 2I_3 + I_5}\right] \tag{1}$$

8-frame 90° [5]
$$\phi = \tan^{-1}\left[\frac{I_1 + 5I_2 - 11I_3 - 15I_4 + 15I_5 + 11I_6 - 5I_7 - I_8}{-I_1 + 5I_2 + 11I_3 - 15I_4 - 15I_5 + 11I_6 + 5I_7 - I_8}\right] \tag{2}$$

9-frame 90° Hibino[6]
$$\phi = \tan^{-1}\left[\frac{\frac{1}{2}(I_1 - 2I_2 - 14I_3 - 18I_4 + 18I_6 + 14I_7 + 2I_8 - I_9)}{I_1 + 4I_2 + 4I_3 - 4I_4 - 10I_5 - 4I_6 + 4I_7 + 4I_8 + I_9}\right] \tag{3}$$

9-frame 90° Phillion[7]
$$\phi = \tan^{-1}\left[\frac{-4I_2 + 12I_4 - 12I_6 + 4I_8}{I_1 - 8I_3 + 14I_5 - 8I_7 + I_9}\right] \tag{4}$$

7-frame 60° [8]
$$\phi = \tan^{-1}\left[\frac{\frac{\sqrt{3}}{3}(-I_1 + 3I_2 + 3I_3 - 3I_5 - 3I_6 + I_7)}{-I_1 - I_2 + I_3 + 2I_4 + I_5 - I_6 - I_7}\right] \tag{5}$$

11-frame 60° Hibino[9]
$$\phi = \tan^{-1}\left[\frac{\sqrt{3}(-I_2 - 4I_3 - 7I_4 - 6I_5 + 6I_7 + 7I_8 + 4I_9 + I_{10})}{2I_1 + 5I_2 + 6I_3 + I_4 - 8I_5 - 12I_6 - 8I_7 + I_8 + 6I_9 + 5I_{10} + 2I_{11}}\right] \tag{6}$$

11-frame 60° Surrel[10]
$$\phi = \tan^{-1}\left[\frac{\sqrt{3}(-I_1 - 2I_2 + 4I_4 + 5I_5 - 5I_7 - 4I_8 + 2I_{10} + I_{11})}{I_1 - 2I_2 - 6I_3 - 4I_4 + 5I_5 + 12I_6 + 5I_7 - 4I_8 - 6I_9 - 2I_{10} + I_{11}}\right] \tag{7}$$

12-frame 60° [10]
$$\phi = \tan^{-1}\left[\frac{\sqrt{3}(-3I_2 - 3I_3 + 3I_4 + 9I_5 + 6I_6 - 6I_7 - 9I_8 - 3I_9 + 3I_{10} + 3I_{11})}{2I_1 + I_2 - 7I_3 - 11I_4 - I_5 + 16I_6 + 16I_7 - I_8 - 11I_9 - 7I_{10} + I_{11} + 2I_{12}}\right] \tag{8}$$

Each of these equations calculates the wrapped phase ϕ where I_i is the irradiance value of the fringe pattern measured for the i-th data frame. The irradiance of the i-th data frame is given by

$$I_i(x,y) = I_o\left\{1 + \gamma\cos\left[\phi(x,y) + a_i'\right]\right\} \tag{9}$$

where I_o is the dc irradiance, γ is the fringe contrast (modulation), $\phi(x,y)$ is the phase being measured and a'_i is the phase shift for the i-th data frame. The algorithms were implemented in Matlab. Fringe data were generated in a spreadsheet.

Errors in the phase shifter motion were modeled assuming

$$a_i' = a_i(1 + ba_i + d) \tag{10}$$

where b is the amount of 2nd-order phase shifter error and d is the linear slope error. When the shifter has no errors, b and d are equal to zero. The phase shifter may both have a slope error due to miscalibration and a nonlinearity. For this study it is assumed that the nonlinearity is of second order. The rough magnitude of this error was determined by measuring phase

shifts on PZT's in an available interferometer. The error terms used in the simulation are estimates of worst-case performance. When phase shifting over 2 waves of OPD it is important to calibrate the slope over the entire throw of the PZT. The presence of a 2nd-order nonlinearity can skew the calibration if it is only done over the 1st wave of OPD shift. Figure 5 shows three different phase shift plots for different amounts of error. In Fig. 5(A) all three are plotted as the actual phase shift versus the desired phase shift with a linear phase shift with no errors as reference. Figure 5(B) shows the error relative to a perfectly linear phase shift. For a phase shift $a'=a(1+0.1a-0.1)$ the phase shifter has 10% nonlinearity and is calibrated so that with one wave OPD of shift, the PZT has the desired phase shift at that point. Note how far off the phase shift can be at 2 waves OPD shift with some nonlinearity present. At 2 waves of OPD, the phase shift is off by 72°. If the same amount of 2nd-order nonlinearity is present and the PZT is calibrated over the 2 waves so that at the 2 wave OPD point the phase shift error is zero, the phase shift would be given by $a'=a(1+0.1a-0.2)$. When the phase shift error is roughly balanced to minimize phase shifter errors, the phase shift can be modeled using $a'=a(1+0.1a-0.125)$. This last case is the one used for the simulations in this paper as a worst case error estimate.

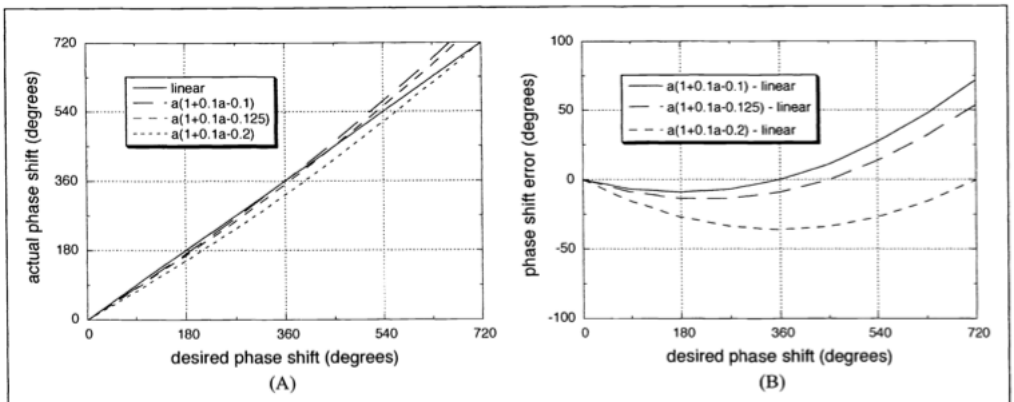

Figure 5. (A). Plot of actual phase shift versus desired phase shift for different motions of the phase shifter. (B). Plot of phase shift error versus desired phase shift for same phase shifter movement as (A).

4. SIMULATION RESULTS

The results of the simulations are shown for a given error and a family of phase measurement algorithms. Figure 6 shows results for the 90° ($\pi/2$) family of algorithms using sinusoidal fringes with a phase shifter motion given by $a'=a(1+0.1a-0.125)$ [note a linear calibrated motion would be $a'=a$]. The algorithm most insensitive to errors in the phase shifter motion is the Schmit/Creath 8-frame with 90° phase shifts [Eq. (2): henceforth referred to in plots as 8fr90]. The algorithm with the largest error is the 5-frame with 90° shifts [Eq. (1): 5fr90]. The other algorithms plotted are the Hibino et al. 9-frame 90° [Eq. (3): 9fr90H] and the Phillion 9-frame 90° [Eq. (4): 9fr90P] which has a much better immunity to phase shifter errors than the 9fr90H algorithm. The peak-to-valley (P-V) for each of the algorithms is shown on the plot. The same phase shifter motion was used to generate the data simulated in Fig. 7 for the 60° ($\pi/3$) family of algorithms. This plot is on the same scale as Fig. 6. Surprisingly the 7-frame 60° algorithm of Larkin and Oreb [Eq. (5): 7fr60] is not the worst performing algorithm for this fringe data. That distinction belongs to the 11-frame 60° algorithm of Hibino et al. [Eq. (6): 11fr60H]. The Surrel 11-frame 60° [Eq. (7): 11fr60S] has a similar performance to the Larkin/Oreb 7fr60 algorithm. The best performing algorithm in this family for this situation by a factor of 10 is the Surrel 12-frame 60° [Eq. (8): 12fr60]. All of these algorithms have an error signature of 2 times the fringe frequency. A more detailed error analysis could be shown, but it is not necessary to see which algorithm performs the best.

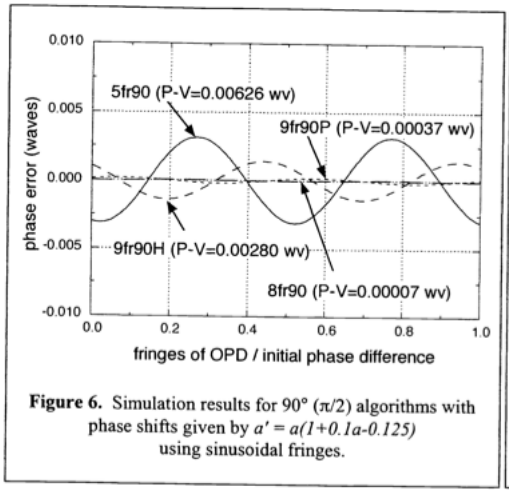

Figure 6. Simulation results for 90° ($\pi/2$) algorithms with phase shifts given by $a' = a(1+0.1a-0.125)$ using sinusoidal fringes.

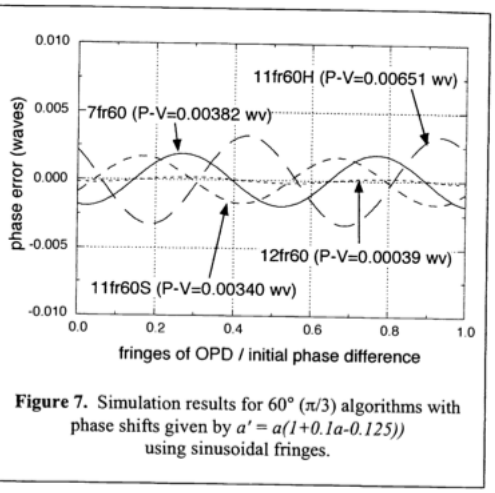

Figure 7. Simulation results for 60° ($\pi/3$) algorithms with phase shifts given by $a' = a(1+0.1a-0.125))$ using sinusoidal fringes.

Next the data from CSIRO for the projected Clapham-Dew interference fringes (Fig. 3) were used as input to the phase measurement algorithms. A front surface reflectance of 2% was assumed as a worst case. Figures 8(A) and (B) show the results for the 2 families of algorithms. All of the 90° algorithms produced the same behavior as did all of the 60° algorithms. It is obvious from the plot that a phase step of 60° greatly improves the performance due to non-sinusoidal fringes. Figure 8(A) is the same scale as Figs. 6 and 7 while Fig. 8(B) has a more sensitive scale to show the detail. The 90° algorithms show an error signature at 4 times the fringe frequency while the 60° algorithms show an error signature at 2 times the fringe frequency.

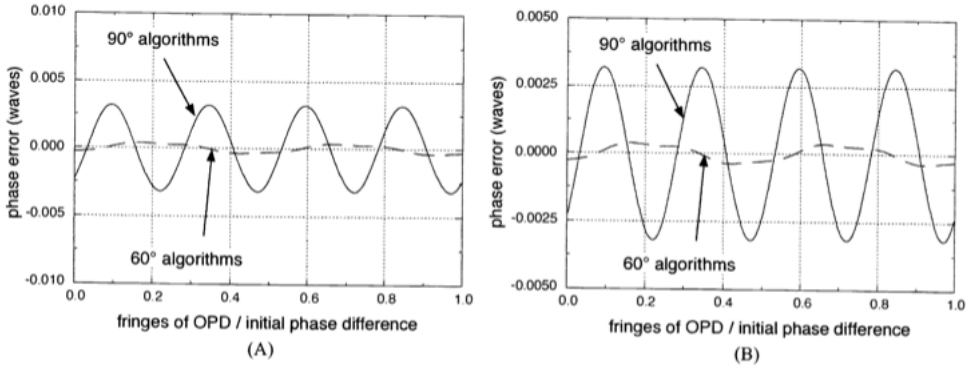

Figure 8. (A). Simulation results showing the effect of the Clapham-Dew coating on the reference surface with a 2% front surface reflectance. Note all 90° ($\pi/2$) algorithms behave the same and all 60° ($\pi/3$) algorithms have a different signature. (B). Same as (A) with a different scale.

Both error sources were combined to determine how the algorithms would behave in a real situation. In general, the algorithms have behaviors that depend upon the coupling of the error sources. The effect of one error can not simply be isolated from another. Figures 9 and 10 shows results for the 90° ($\pi/2$) and 60° ($\pi/3$) families of algorithms. As expected from the previous results, the 60° family of algorithms is less sensitive to the error due to the non-sinusoidal fringes. However, the behavior of the different algorithms varies significantly when both errors are present. There are 2 algorithms - the 11fr60S and the 12fr60 - that have sufficient performance for this application. The difference between the algorithms is one frame of data. The 12th frame of data gains an extra factor of 2 in performance. Thus it is possible to have a P-V error of 2 thousandths of a wave due to anticipated errors in the phase shifter and non-sinusoidal fringes. This level of error performance leaves the major measurement challenges to be environmental.

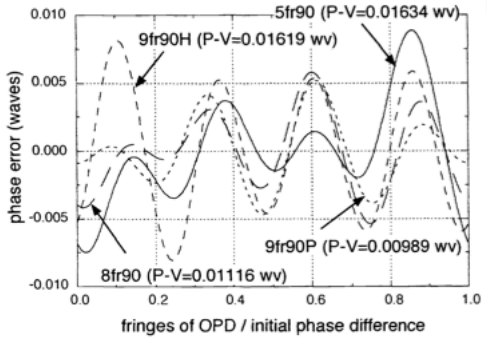

Figure 9. Simulation results for 90° ($\pi/2$) algorithms with phase shifts given by $a' = a(1+0.1a-0.125)$ showing the effect of the Clapham-Dew coating on the reference surface with a 2% front surface reflectance.

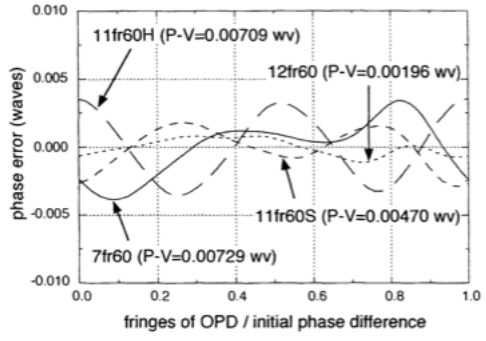

Figure 10. Simulation results for 60° ($\pi/3$) algorithms with phase shifts given by $a' = a(1+0.1a-0.125)$ showing the effect of the Clapham-Dew coating on the reference surface with a 2% front surface reflectance.

The results of the simulations are summarized in Figs. 11 and 12. Figure 11 shows plots of the 8-frame 90° algorithm for the phase shifter error (labeled uncalibrated), the non-sinusoidal fringes due to Clapham-Dew type coating and the combination of the 2 errors. The relative amplitudes of the different cases and the behavior of the algorithm when both errors are present can clearly be seen. Figure 12 shows the plots for the 12-frame 60° algorithm with the same error sources as Fig. 11. Note that the vertical scale of Fig. 12 is 5 times more sensitive than that of Fig. 11. Rather than having ripple at 4 times the fringe frequency as the 8-frame 90° algorithm shows, the 12-frame 60° algorithm has a more complex signature. The dominant term is at twice the fringe frequency. However, as the scale has been blown up to see the detail, this error is not expected to be the limiting factor in making measurements.

From the results of the simulations it was decided to use the 8-frame 90° algorithm with uncoated surfaces and the 12-frame 60° algorithm with coated surfaces. The main reason for deciding to use 2 different algorithms was that whenever fewer frames of data can be taken the faster the measurements can be made thereby reducing environmental variations. These sorts of variations include such factors as temperature and humidity variations, air turbulence or acoustical coupling.

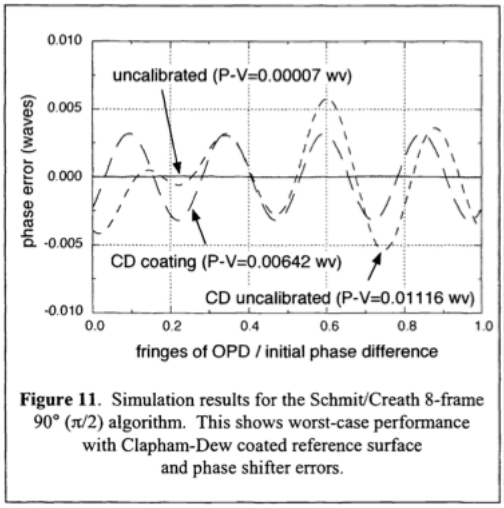

Figure 11. Simulation results for the Schmit/Creath 8-frame 90° ($\pi/2$) algorithm. This shows worst-case performance with Clapham-Dew coated reference surface and phase shifter errors.

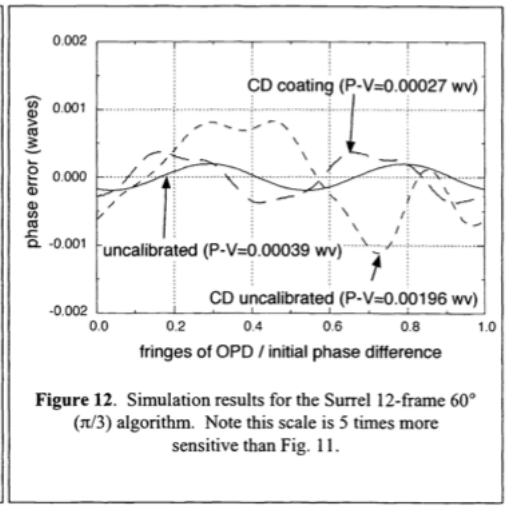

Figure 12. Simulation results for the Surrel 12-frame 60° ($\pi/3$) algorithm. Note this scale is 5 times more sensitive than Fig. 11.

5. MEASUREMENTS OF "REAL" SURFACES

Figures 13 and 14 shows measurements with the Wyko 6000 interferometer of a LIGO high reflectance surface versus the Clapham-Dew coated reference flat. The test surface was curved and there were 2 fringes of tilt present. These data show phase maps of single measurements where the interferometer has not been adjusted between data sets other than to change the phase-measurement algorithm and scale the PZT shift. The PZT was calibrated over the 1st full wave of OPD of the shifter range. No averaging was done. No reference surface was subtracted. Tilt, power, astigmatism, coma and spherical aberration were subtracted to better compare the ripple. Finally the two plots were scaled to have the same height scales. The 8-frame 90° algorithm shows noticeably more ripple than the 12-frame 60° algorithm. The 8-frame 90° algorithm shows a residual error at 4 times the fringe frequency. It is obvious that the ripple has almost as large an amplitude as the height scale. The height scale is 1/100th of the 1064 nm wavelength. Although this may seem like a small number, the structure on the test surface of interest is even smaller. For comparison, Fig, 14 shows the results of the 12-frame 60° algorithm. There is much less error present. The ripples have a smaller amplitude and more structure can be seen in the phase map that can be attributed to either the reference or test surfaces. Because the test surfaces have rms roughnesses on the order of 1 nm or less, it is important to reduce as much error as possible. The residual ripple seen in Fig. 14 can further be reduced by averaging many consecutive measurements. In practice, 8 sets of data are averaged and saved and this is done 10 times in a row with as little time between measurements as possible. Since the phase of the ripple depends upon the initial phase of the first interferogram captured, averaging can further be enhanced by either adding an extra phase step between measurements to ensure a different initial phase[2] or by adding some air turbulence to randomize the initial phase.[16] Both methods have been shown to improve the measurement results on uncoated surfaces and to help reduce environmental effects.

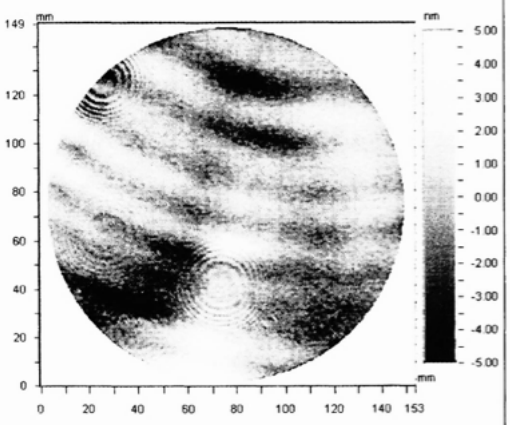

Figure 13. Measurement of a high reflectance surface using the 8-frame 90 algorithm with a Clapham-Dew coated reference surface. Note ripple at 4x the fringe frequency.

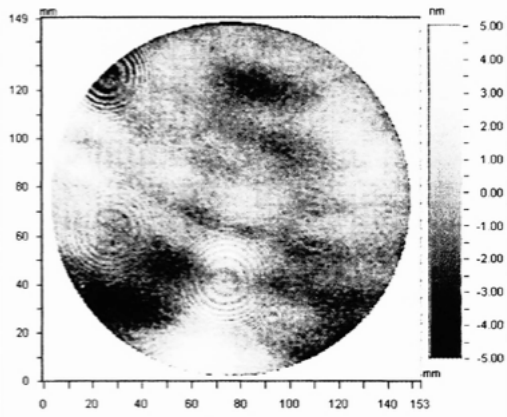

Figure 14. Measurement with same surfaces as Fig. 13 without adjusting fringes, and on same scale using the 12-frame 60 algorithm. Note much less ripple.

6. CONCLUSIONS

Utilizing phase-measurement algorithms that use data over a larger range of phase shifter motion can help reduce the effects of errors when measuring high reflectance surfaces where the fringes may be non-sinusoidal. Even if linear and 2nd-order phase shifter errors are present, the added frames of irradiance data can aid in making a better estimate of the phase. Algorithms have been designed to specifically reduce these types of errors. Eight algorithms that have been published in the literature where compared using simulations and with experimental measurements. From this study, the algorithms that work the best are the 8-frame 90° algorithm for uncoated test and reference surfaces, and the 12-frame 60° algorithm for use with Clapham-Dew coated reference surfaces and high reflectance test surfaces. Errors due to residuals in the phase calculation can be reduced down to a few thousandths of a wave P-V.

ACKNOWLEDGEMENTS

The author wishes to acknowledge GariLynn Billingsley, Michael Hrynevych, Jordan Camp and Stan Whitcomb of the LIGO project for their support of this project. To Erik Novak, Joe Lamb and Paul Unruh et al. of Veeco Process Metrology for their help implementing these techniques. Additional thanks to Chris Walsh, Roger Netterfield, Bob Oreb and David Farrant of CSIRO, Chris Evans of NIST and Bob Parks and Lianzhen Shao of the Optical Perspective Group for sharing their knowledge of measuring high precision optical surfaces.

This material is based upon work supported by the National Science Foundation under the Co-operative Agreement with the California Institute of Technology, No. PHY-9210038.

REFERENCES

1. G. Billingsley,"Gravitational wave interferometry: how does it work?," *Proc. SPIE* **3744** 2-10 (1999).
2. C.J. Walsh, A.J. Leistner, J. Seckold, B.F. Oreb and D.I. Farrant, "Fabrication and Measurement of Optics for LIGO," *Appl. Opt.* **38**(13) 2870-2879 (1999).
3. D.I. Farrant, A.J. Leistner, B.F. Oreb, M.A. Suchting and C.J. Walsh, "Metrology of LIGO pathfinder optics," *Proc. SPIE* **3134** 79-85 (1997).
4. P.B. Clapham and G.D. Dew, "Surface-coated reference flats for testing fully aluminized surfaces by means of the Fizeau interferometer," *J. Sci. Instrum.* **44,** 899-902 (1967).
5. J. Schmit and K. Creath, "Window function influence on phase error in phase-shifting algorithms," *Appl. Opt.* **35** (28), 5642-5649 (1996).
6. K. Hibino, B. F. Oreb, D. I. Farrant *et al*., "Phase-shifting algorithms for nonlinear and spatially nonuniform phase shifts," *J. Opt. Soc. Am. A* **14** (4), 918-930 (1997).
7. D. W. Phillion, "General methods for generating phase-shifting interferometry algorithms," *Applied Optics* **36** (31), 8098-8115 (1997). *[Note that the 9-frame 90° algorithm used in this study differs slightly from the one in Phillion's paper. The coefficients for this algorithm were provided by Phillion.]*
8. K. G. Larkin and B. F. Oreb, "Design and assessment of symmetrical phase-shifting algorithms," *J. Opt. Soc. Am. A* **9** (10), 1740-1748 (1992).
9. K. Hibino, B. F. Oreb, D. I. Farrant *et al*., "Phase shifting for nonsinusoidal waveforms with phase-shift errors," *J. Opt. Soc. Am. A* **12** (4), 761-768 (1995).
10. Y. Surrel, "Additive noise effect in digital phase detection," *Appl. Opt.* **36**(1) 271-276 (1997). *[Note there are typographic errors in algorithms (17) and (19) of Table 1.]*
11. P. S. Fainman, et al., "300-nm-aperture phase-shifting Fizeau interferometer," *Opt. Eng.* **38**(08) 1371-1380 (1999).
12. P. Hariharan, "Optical flat surfaces: direct interferometric measurements of small-scale irregularities," *Opt. Eng.* **35**(11) 3265-3266 (1996).
13. P. Hariharan, "Interferometric measurements of small-scale surface irregularities: sources of error," *Opt. Eng.* **36**(8) 2330-2334 (1997).
14. P. Hariharan, "Interferometric testing of optical surfaces: absolute measurements of flatness," *Opt. Eng.* **36**(9) 2478-2481 (1997) and C.J. Evans, "Comment on the paper "Interferometric testing of optical surfaces: absolute measurements of flatness"," *Opt. Eng.* **37**(6) 1880-1882 (1998).
15. D. I. Farrant et al., "Metrology of LIGO pathfinder optics," *Proc. SPIE* **3134** 79-85 (1997).
16. R.E. Parks, C.J. Evans, P.J. Sullivan, L.-Z. Shao and B. Loucks, "Measurements of the LIGO pathfinder optics," *Proc. SPIE* **3134** 95-111 (1997).
17. R.P. Bourgeois, J. Magner and H. P. Stahl, "Results of the calibrations of interferometer transmission flats for the LIGO pathfinder optics," *Proc. SPIE* **3134** 86-94 (1997).
18. K. Creath, "Precision measurement of high reflectance LIGO surfaces," in preparation.
19. B. F. Oreb et al., "Metrology of LIGO core optics," *Proc. SPIE* **3744** 18-30 (1999).
20. C. J. Walsh et al., "Metrology of transmission optics for LIGO," *Proc SPIE* **3745** 331-339 (1999).
21. C. J. Walsh et al., "Manufacture of LIGO core optics at CSIRO," *Proc. SPIE* **3782** 214-223 (1999).
22. R. P. Netterfield et al., "Coating requirements for the reference flat of a Fizeau interferometer used for measuring from uncoated to highly reflecting surfaces," *Proc. SPIE* **3738** 128-135 (1999).
23. B. F. Oreb et al., "Characterization of wavefront variations in coated optics," *Proc SPIE* **3782** 232-243 (1999).
24. Simulated interference fringe data provided by Roger Netterfield of CSIRO.
25. J. Schwider, R. Burow, K. E. Elssner *et al*., "Digital wave-front measuring interferometry: some systematic error sources," *Applied Optics* **22** (21), 3421-3432 (1983).
26. P. Hariharan, B. F. Oreb and T. Eiju, "Digital phase-shifting interferometry: a simple error-compensating phase calculation algorithm," *Applied Optics* **26** (3), 2504-2505 (1987).